SCIENCE CHINA
Technological Sciences

•Article•

September 2019 Vol.62 No.9: 1534–1544
https://doi.org/10.1007/s11431-018-9412-1

Modelling of dynamic recrystallization kinetics of 300M steel at high strain rates during hot deformation

GUO Peng, DENG Lei, WANG XinYun* & LI JianJun

State Key Laboratory of Materials Processing and Die & Mould Technology, Huazhong University of Science and Technology, Wuhan 430074, China

Received August 30, 2018; accepted December 14, 2018; published online May 5, 2019

The flow curves of 300M steel exhibit a transition from stress peak presence to stress peak absence as the strain rate increases. It is difficult to establish dynamic recrystallization (DRX) kinetics models suitable for strain rates where there are no stress peaks in the flow curves using the existing Avrami equation, and the optimal processing parameters for forging can be scarcely acquired. In this study, the high-temperature flow and DRX behavior of 300M steel are investigated by performing isothermal compression tests at temperatures between 1173–1423 K with strain rates between 0.001–50 s^{-1}. Distinct stress peaks can be found in the flow curves at low strain rates, and the average grain size decreases with the increase in the strain rate at the same temperature. The DRX mechanism is a discontinuous DRX, and the grain boundary migration plays an important role in the DRX process. In contrast, no stress peak is observed in the flow curves at high strain rates, and the average grain size no longer decreases with the strain rate increase at the same temperature. The DRX mechanism in this case is a continuous DRX. The demarcated strain rate is calculated based on the characteristics of the obtained flow curves and grain sizes. The recrystallization volume fraction model and prediction grain size model at high strain rates are established. In combination with the existing DRX kinetics models at low strain rates, the processing parameters can be optimized to produce components with excellent mechanical properties.

300M steel, flow curves, demarcated strain rate, dynamic recrystallization, grain size

Citation: Guo P, Deng L, Wang X Y, et al. Modelling of dynamic recrystallization kinetics of 300M steel at high strain rates during hot deformation. Sci China Tech Sci, 2019, 62: 1534–1544, https://doi.org/10.1007/s11431-018-9412-1

1 Introduction

Metals and alloys typically undergo work hardening (WH), dynamic recovery (DRV), and dynamic recrystallization (DRX) during hot deformation [1–4]. Among these processes, DRX will cause softening of the materials, result in grain refinement, and improve the mechanical properties of the materials [5–7]. However, DRX is an extremely complex process and closely related to the hot processing parameters, particularly the strain rate. Therefore, studying the effect of the deformation parameters on the DRX behavior is beneficial for optimizing the processing parameters, which can provide components with favorable mechanical properties.

A medium-carbon and low-alloy ultrahigh strength steel, 300M, is modified by adding 1.6 wt.% silicon and 0.1 wt.% vanadium in 4340 steel. Owing to its excellent properties such as high strength, preferable fracture toughness, and strong stress corrosion resistance, 300M steel parts have been widely used in heavy load-bearing components, such as aircraft landing gears and flap main tracks [8,9]. The mechanical properties of these components are significantly affected by the hot processing parameters. Recently, some studies have been conducted on the flow and DRX behavior of 300M steel to improve the mechanical properties of components by the hot working process [10–12]. Luo et al. [8] and Liu et al. [13] studied the flow behavior and mi-

*Corresponding author (email: wangxy_hust@163.com)

crostructure evolution of 300M steel at various temperatures and strain rates by isothermal compression tests. Luo et al. [8] reported that no stress peak was observed in the flow curves at strain rates ranging from 10 s^{-1} to 1 s^{-1}, and that DRV was the dominant softening mechanism. Liu et al. [13] mentioned that a stress peak was present at strain rates lower than 1 s^{-1}, indicating that 300M steel underwent a discontinuous DRX (DDRX) process. Based on the Avrami equation, they built the DRX volume fraction model, which was only suitable for a flow curve with a stress peak at a low strain rate owing to the inclusion of the peak strain in the model. The hot flow behavior and microstructure evolution of 300M steel mentioned above indicates that 300M steel exhibits different flow behaviors and DRX mechanisms in the high and low strain rate regions. This phenomenon is also be found in other materials [14–19]. Thus, precisely demarcating the high and low strain rate regions is crucial for the accurate modeling of the DRX kinetics and ideal optimization of the hot processing parameters. However, still there has been no study attempting to distinguish the strain rate regions. Although the highest strain rate that can be reached during the forging of 300M steel is 50 s^{-1}, still there are no accurate DRX kinetics models suitable for such high strain rates. Therefore, it is usually very difficult to obtain the optimized processing parameters, and thus, formation of defects, such as coarse grains and inhomogeneous microstructures, frequently occurs. Hence, the mechanical properties including the strength and toughness, as well as the service life of 300M steel components are significantly reduced.

In the present work, the flow behavior and DRX mechanism of 300M steel under different forming conditions were investigated by performing isothermal compression tests. A method combining the stress ratio with the grain size was proposed to calculate the demarcated strain rate (DSR). Subsequently, the occurrence mechanism of flow curves with/without stress peaks was analyzed. Finally, the DRX volume fraction model and grain size model at high strain rates were established.

2 Materials and methods

The chemical composition (wt.%) of the as-received 300M steel is as follows: 0.38 C, 0.74 Mn, 1.64 Si, 1.87 Ni, 0.84 Cr, 0.08 V, 0.40 Mo and Fe to balance the weight percentage. The average grain size is 31.2 μm (see Figure 1(a)). Compression specimens with a diameter of 8 mm and height of 12 mm were machined from the as-received 300M by wire cutting along the circumferential direction to ensure the consistency of the original microstructure of the specimens. Forming temperatures were selected from 1173 K to 1423 K with an interval of 50 K. The highest strain rate is approximately 50 s^{-1} in the pre-forming process performed by a C5T electro-hydraulic hammer, and the lowest strain rate is typically approximately 0.001 s^{-1} in the final forming process conducted by a die-forging hydraulic press. Therefore, in this study, the strain rates were set as 0.001, 0.01, 0.1, 1, 3, 10 and 50 s^{-1}. In contrast, as the strains of the forged parts often range from 0 to 1.2 in the different sections, in the experiments, strains of 0.10, 0.22, 0.36, 0.50, 0.69, and 1.2 were chosen. The specimens were heated to the desired temperature at a rate of 5 K/s and held for 4 min to obtain a uniform temperature field distribution. Isothermal compression tests were conducted on a GLEEBLE-3500 thermal simulator by following the experimental procedure illustrated in Figure 1 (b). The specimens were compressed under the selected strain rate and quenched by water immediately. The water was sprayed on the specimen after 0.24 s (0.1 s for power-off and 0.14 s for delay of the quenching process) of the deformation. Then the temperature was dropped to *Ms* (570 K for 300M steel) at 0.46 s and stabilized below 353 K within 2 s. To acquire the initial microstructure before the deformation, some specimens were heated to the deformation temperatures at a heating rate of 5 K/s and held for 4 min, and were quenched by water immediately without deformation. It is well known that 300M steel undergoes a phase transition from austenite to martensite during quenching. The structure observed at room temperature is martensite. Refs. [20–22] showed the grain boundary obtained by chemical etching of the martensite structure using a specific chemical etchant was the prior-austenite grain boundary. The phase transition only changes the orientation and has no effect on the prior-austenite grain size. To acquire the prior-austenite grain size, after compression the specimens were sectioned along the direction of compression and etched at room temperature by saturated picric acid aqueous solution, CCl_4, detergent, and HCl (5:1:1:0.01) after metallurgical polishing. The microstructures were observed using an OLYMPUS BX61 optical microscope, and the average austenite grain size was measured by the linear intercept method [23].

3 Results

3.1 Flow curves and microstructures

The flow curves at different temperatures and strain rates are shown in Figure 2, exhibiting obvious differences between the flow curves. At the strain rate of 0.01 s^{-1} (see Figure 2 (a)), the flow curves at various temperatures show distinct stress peaks, indicating that 300M steel undergoes DDRX [24–26]. However, at the strain rate of 10 s^{-1} (see Figure 2 (b)), the flow stress monotonically increases with the strain increase and tends to be steady in the end, with no stress peak observed at all the temperatures. The change in the flow

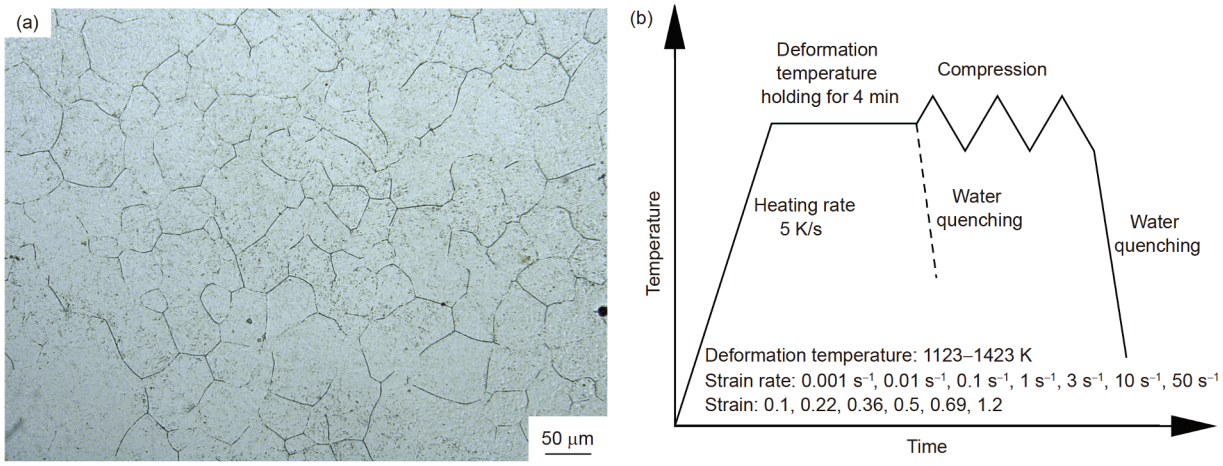

Figure 1 The as-received microstructure and experimental procedure: (a) microstructure of as-received 300M steel; (b) experimental procedure.

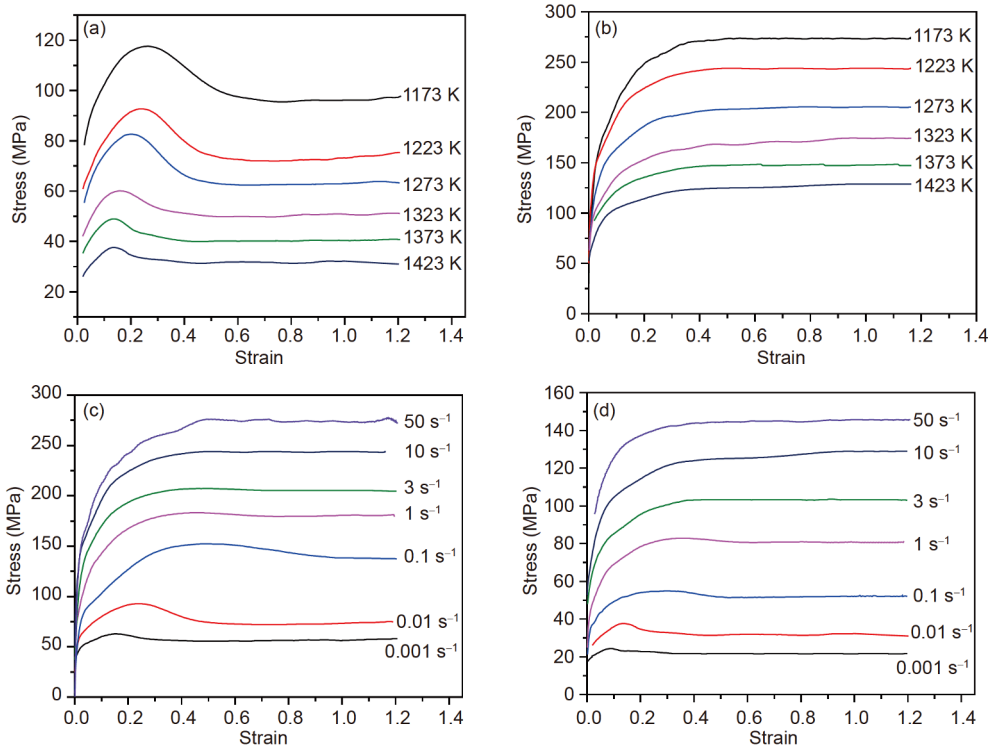

Figure 2 Flow curves under various deformation conditions: strain rates of (a) 0.01 s^{-1}; (b) 10 s^{-1}; temperatures at (c) 1223 K; (d) 1423 K.

curves from with-stress-peak to without-stress-peak indicates that the flow behavior and DRX mechanism of 300M steel change with increasing strain rate [27]. The comparison of Figure 2(a) and (b) shows that the strain rate has more obvious effects on the flow behavior of 300M steel than those of temperature. It can be found from Figure 2(c) and (d) that at all the temperatures, the flow curves exhibit a transition from with-stress-peak to without-stress-peak with the increase in the strain rate. Moreover, there is a DSR between 1 and 3 s^{-1}. The precise determination of the DSR will be described in Sect. 3.2.

The microstructures of the initial and deformed 300M steel at different strain rates and 1423 K are shown in Figure 3. It can be seen that after deformation, the microstructures notably differ from the initial structure, both in terms of the morphology and grain size. This difference is attributed to the occurrence of DRX. In addition, the occurrence of the variation in the grain shapes and grain boundaries occurs with strain rate increase. At strain rates of 0.01, 0.1 and 1 s^{-1}, most of the grains are irregularly equiaxed with the curved grain boundaries, implying that grain boundary migration occurs during this process. Moreover, it is observed that the

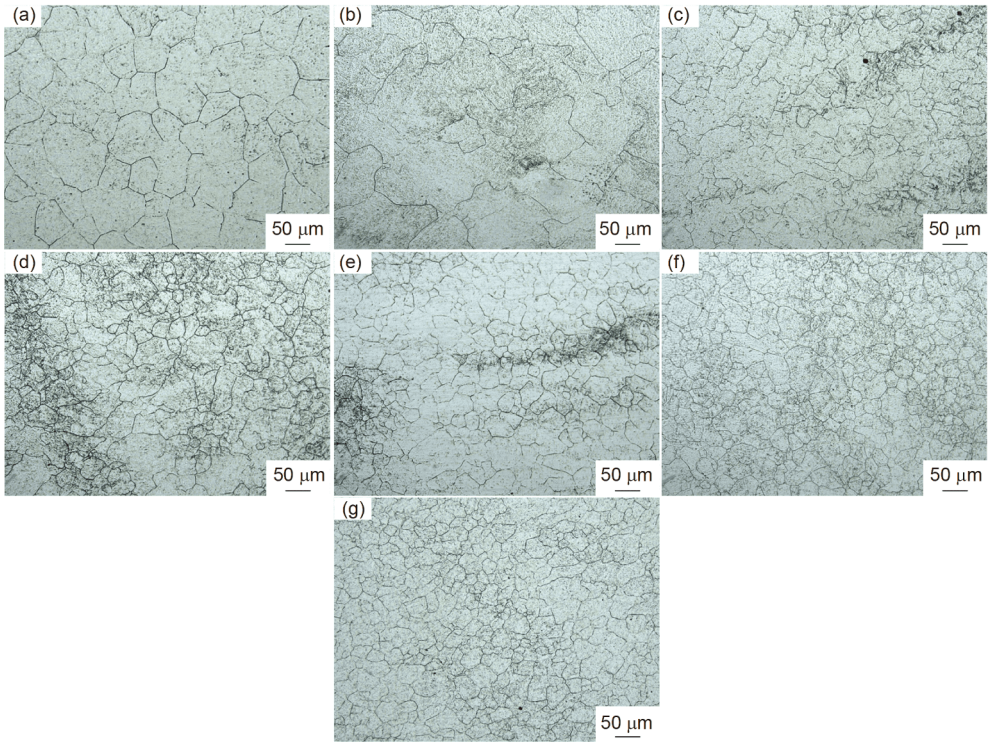

Figure 3 (Color online) Microstructures at 1423 K, (a) initial microstructure; deformed at strain of 1.2 when the strain rate is: (b) 0.01 s^{-1}; (c) 0.1 s^{-1}; (d) 1 s^{-1}; (e) 3 s^{-1}; (f) 10 s^{-1}; (g) 50 s^{-1}.

average grain size decreases with the strain rate increase. However, when the strain rates are 3, 10 and 50 s^{-1}, most grains are regularly equiaxed with the relative straight grain boundaries, whereas the average grain size remains almost unchanged with the increase in the strain rate.

3.2 Determination of DSR

It is described in Sect. 3.1 that an obvious transition occurs in both the flow curves and grain sizes as the strain rate increases. Therefore, the DSR can be calculated based on the transition. The ratio of the peak stress (σ_p) to the steady stress (σ_s) is used and shown in Figure 4(a). The ratio is higher than 1 at strain rates of 0.01, 0.1 and 1 s^{-1}, owing to the existence of the stress peak, whereas the ratio is 1 at strain rates of 3, 10 and 50 s^{-1}, attributing to the absence of the stress peak. A linear equation can be obtained via linear fitting of the points at a ratio higher than 1 and be used to acquire the DSR, which is 1.75 s^{-1} when the ratio drops to 1. Considering the fluctuation in the flow stress caused by friction, the ratio of the peak stress to the stress at a strain of 1.2 ($\sigma_{\varepsilon_{1.2}}$) is also used (see Figure 4(b)), and the calculated DSR is 1.89 s^{-1}. In addition, the DSRs obtained by combining the linear equations acquired by the grain sizes at strain rates lower than 1 s^{-1} and higher than 3 s^{-1} are denotes as the hollow symbols in Figure 4(c), i.e., curves for 1.67, 1.75 and 1.82 s^{-1} at 1223, 1323 and 1423 K, respectively. There is good correspondence with the DSRs 1.75 s^{-1} and 1.89 s^{-1} obtained based on the transition of the flow stress, indicating that there is a close relation between the microstructure evolution and flow behavior. Based on the above results, the DSR of 300M steel is determined as 1.8 s^{-1} after averaging. In this paper, strain rates below 1.8 s^{-1} are defined as low strain rates, otherwise they are defined as high strain rates.

4 Discussion

4.1 Differences between flow curves

4.1.1 Flow curves with stress peak at low strain rate

The flow curve and microstructures at 1323 K and 0.1 s^{-1} are displayed in Figure 5. It can be seen that the grain boundaries obviously bulge at low strains. As the strain increases, DRX nuclei are formed at the original grain boundaries and grow into DRX grains. The DRX process completes when the DRX grains replacing all the initial grains, and the average grain size reaches a steady value. The DRX mechanism is DDRX, which is a process of nucleation and grain growth [28].

When deforming at a low strain rate, serrated boundaries are developed because of the incompatibility in the grains. The fluctuations prevent further grain boundary sliding, leading to the accumulation of dislocations [27]. When the dislocation density reaches a critical value the dislocation

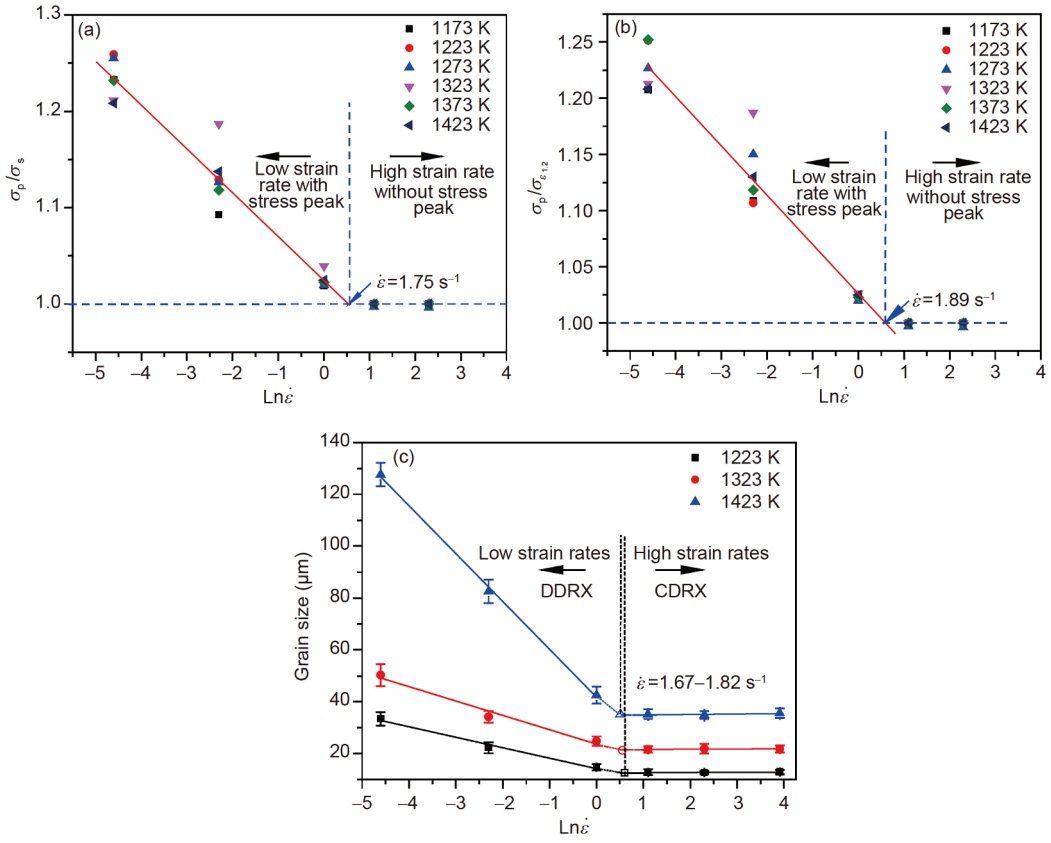

Figure 4 Relation between: (a) σ_p/σ_s and the strain rate; (b) $\sigma_p/\sigma_{\varepsilon 12}$ and the strain rate; (c) the grain size and strain rate.

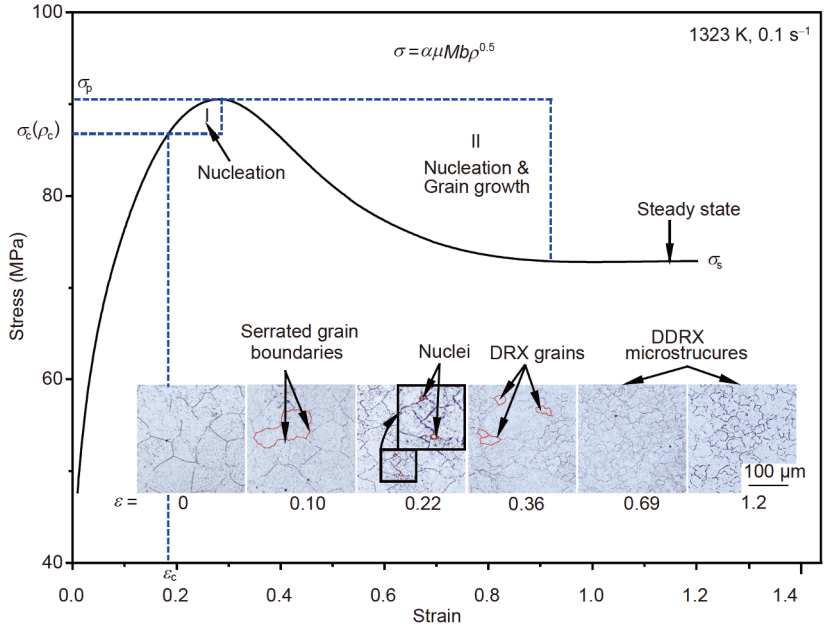

Figure 5 Flow curve and microstructures at 1323 K and 0.1 s^{-1}, the red lines indicate the grain boundaries.

density gradient is sufficiently large, DRX nuclei are formed at the original grain boundaries. Subsequently, the long-range migration of the grain boundaries leads to grain growth, which consumes many dislocations and decreases the dislocation density [24]. The flow stress of region I in Figure 5 is higher than the DRX critical stress (the DRX

critical stress corresponds to the DRX critical strain, which is the strain at which DRX begins [1]). Therefore, the dislocation density is higher than the critical dislocation density based on the relation of flow stress σ and average dislocation density $\bar{\rho}$: $\sigma = \alpha\mu M\mathbf{b}\sqrt{\bar{\rho}}$ [29]. Here, α is a constant, μ is the shear modulus, M is the orientation factor, and b is Burgers vector. Hence, region I is the region of nucleation. The grain boundary migration rate can be expressed as follows [30]:

$$v = \frac{\mathbf{b}\delta D_{0\mathrm{b}}}{K_{\mathrm{B}}T}\exp\left(-\frac{Q_{\mathrm{b}}}{RT}\right)\left[\tau(\rho_m - \rho_0) - \frac{2\gamma_m}{r}\right]. \quad (1)$$

In eq. (1), δ is the thickness of the grain boundary, $D_{0\mathrm{b}}$ is the boundary self-diffusion coefficient at 0 K, Q_{b} is the diffusion activation energy, K_{B} is the Boltzmann constant, R is the gas constant, T is the temperature, τ is the dislocation line energy, γ_m is the grain boundary energy, and r is the radius of grain. It can be found from eq. (1) that the driving force is small when r is small, resulting in a low migration rate of the grain boundaries. The size of the nuclei forming in region I is relatively small (see the microstructure of $\varepsilon = 0.22$ in Figure 5); therefore, the migration distance is very short and practically no grain growth occurs in this region. Thus, few dislocations are consumed by the grain boundary migration, and the dislocations consumed by DRV and DRX cannot compensate the dislocations generated by deformation, leading to an increase in the dislocation density. Thus, the flow stress still increases in region I, which exhibits that WH is macroscopic. In region II in Figure 5, not only does nucleation occur in the material but also the grain growth (see the microstructures from $\varepsilon = 0.22$ to $\varepsilon = 0.36$ in Figure 5) caused by the grain boundary migration. Among the two, the grain growth is more important. In this process, the region swept by the grain boundaries gradually increases. Thus, numerous dislocations generated by the deformation are absorbed. The number of dislocations consumed by DRV and DRX is larger than that generated by deformation, resulting in a decrease in the average dislocation density. Accordingly, the flow stress decreases with strain increase. The initial grains are gradually substituted by the growing DRX grains, and when the DRX grains replace all the initial grains, DRX completes. At this stage, only local nucleation and grain growth occur, and there is a balance between the softening caused by the DRV and DRX processes and the WH induced by the deformation, so that the flow curves plateau. The grain boundary migration plays an important role in DDRX. In the DRX process, the DRX nuclei grow into DRX grains via grain boundary migration and consume numerous dislocations, decreasing the average dislocation density. At the macro level, the flow stress first increases and then decreases to a steady stress, i.e., stress peaks are observed in the flow curves. The deformation time becomes shorter with the increase in the strain rate, and the migration distance reduces, leading to a decrease in the number of dislocations consumed by the grain boundary migration correspondingly. The ratio of the peak stress to steady stress gradually decreases to 1 with the increase in the strain rate (see Figure 4(a)).

4.1.2 Flow curves without stress peak at high strain rate

The flow curves at high strain rates exhibit characteristics that are different from those at low strain rates. No stress peak is observed at high strain rates, and the flow stress increases with the strain monotonously and finally tends to stabilize. Figure 6 shows the flow curve and microstructures obtained at 10 s^{-1} and 1323 K. It can be seen that there is no

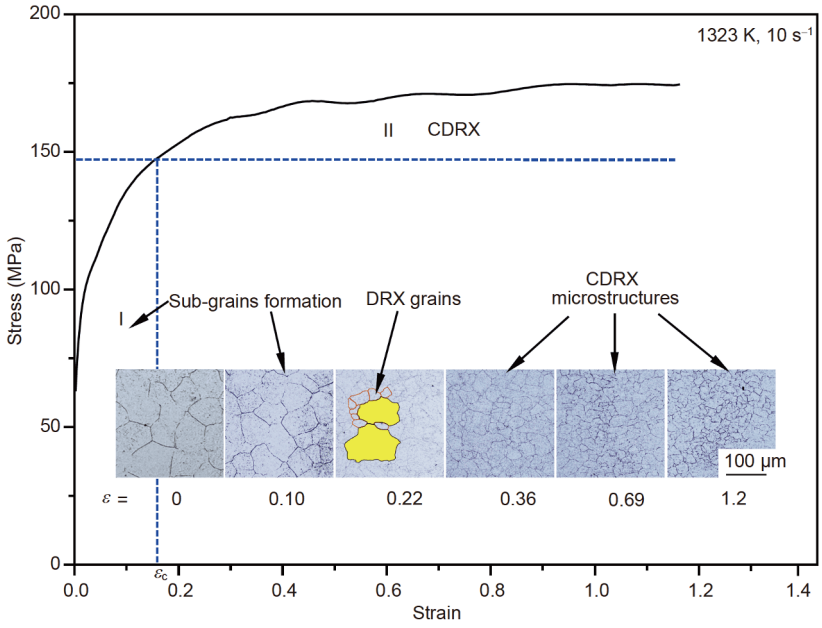

Figure 6 Flow curve and microstructures at 1323 K and 10 s^{-1}. The red lines are the grain boundaries and the yellow zones are the initial grains.

grain boundary bulging or nucleation at a low strain (ε=0.1). In addition, the morphology of the microstructure and average grain size are practically the same as those of the initial microstructure. These phenomena are different from the characteristics at low strain rates. New regularly equiaxed grains with finer sizes are formed at the original grain boundaries with the increase in the strain (see the grains marked by red lines in Figure 6, and the yellow zones are the initial grains). Limited by the deformation time, these new DRX grains do not grow with the increase in the strain, so that the average size of the DRX grains is practically the same as that of the grains at the strain of 1.2 (see d_{DRX} in Figure 7). Here, the average size of the DRX grains is determined by the linear intercept method applied to the regularly equiaxed grains that are smaller than half of the average size of the initial grains; these grains can be regarded as the new DRX grains. Compared with the DRX mechanism at low strain rates, it can be found that the DRX mechanism at high strain rates is not a DDRX but a continuous DRX (CDRX).

Region I in Figure 6 is the initial state of the deformation, in which the formation of new grains does not occur, but the dislocations generated by the deformation form sub-grains [31,32]. With a continuous input of deformation energy, the misorientation of the sub-grains gradually increases. The sub-grain boundaries transform into high-angle grain boundaries and form new grains when a critical strain is reached. Region II arises from new grains being continuously formed through the transformation of the low-angle sub-grain boundaries into high-angle grain boundaries.

During the deformation process at high strain rates, the critical resolved shear stress is relatively higher than that a low strain rate, causing the slip system opening and grain boundaries sliding to be difficult. Thus, local shearing first occurs near the original grain boundaries, leading to local non-uniform deformation [33]. New fine grains form at the original grain boundaries by progressive lattice rotation. The average size of the grains so formed is simply related to the temperature and has no correlation to the strain rate (see Figure 4(c)). Grain boundary migration does not occur place in this relatively short time, and consequently, the DRX grain size remains constant with the increase in the strain rate and strain, and the flow curve does not exhibit any stress peak.

4.2 Modeling of DRX kinetics models at high strain rate

4.2.1 Modeling of DRX volume fraction

During high-strain rate deformation, average size of the DRX grains d_{DRX} remains constant with the increase in the strain at the same temperature, and average size of all the grains d_{avg} has no correlation with the strain rate (see Figure 7). Based on this, the DRX volume fraction can be established by a series of grain sizes, namely, d_0, d_{DRX}, and d_{avg}. Here, d_0 is the initial grain size of the initial microstructure before deformation. Figure 8 presents a schematic of the mathematical model developed to describe the volume fraction of DRX at high strain rates. It is supposed that there are n initial grains of size d_0 in length l. At strain ε, n_1 DRX grains with average size d_{DRX} are formed, and the initial grain size becomes d_1. Accordingly, eq. (2) can be derived as

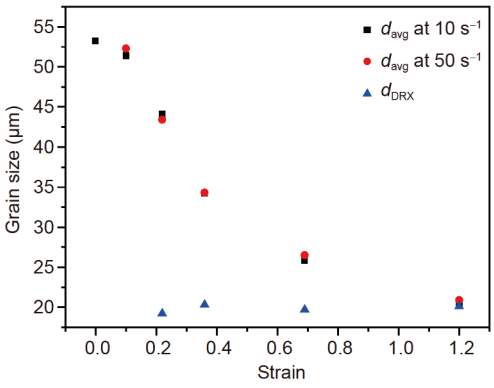

Figure 7 (Color online) Relation between the average size of the DRX grains (d_{DRX}) and average size of the all grains (d_{avg}) at 1323 K and 10 s^{-1}, 50 s^{-1}.

$$l = n \cdot d_0 = n_1 \cdot d_{DRX} + n \cdot d_1 = (n_1 + n) \cdot d_{avg}. \quad (2)$$

When d_1=d_{DRX}, there is d_{avg}=d_{DRX}, which means the DRX completes. Then, X_{DRX} is built as

$$X_{DRX} = \frac{d_{DRX}}{d_0 - d_{DRX}} \cdot \left(\frac{d_0}{d_{avg}} - 1 \right). \quad (3)$$

4.2.2 Modelling of grain sizes

Because the DRX grain size during deformation simply correlates to the temperature and has hardly related to the strain rate under the experimental conditions of high strain rate mentioned earlier, both d_0 and d_{DRX} can be expressed by a type of Arrhenius equation as follows:

$$d = C \cdot \exp(-\beta Q / RT), \quad (4)$$

where C is a material constant, β is the correction coefficient, and Q is the activation energy. Figure 9(a) displays the relation between d_0 and Q_{GG}/RT, where Q_{GG} is the grain growth activation energy, 132 kJ/mol for 300M steel [23]. Figure 9(b) shows the relation between d_{DRX} and Q_D/RT, where Q_D is the deformation activation energy, 381.34 kJ/mol [13]. It can be found from Figure 9(a) and (b) that there is a good linear relation between the grain sizes and Q_{GG}/RT or Q_D/RT, and the former can be expressed as follows:

$$\begin{cases} d_0 = 3.83 \times 10^3 \cdot \exp\left(-0.3567 \cdot \dfrac{Q_{GG}}{RT}\right), \\ d_{DRX} = 1.51 \times 10^4 \cdot \exp\left(-0.1899 \cdot \dfrac{Q_D}{RT}\right). \end{cases} \quad (5)$$

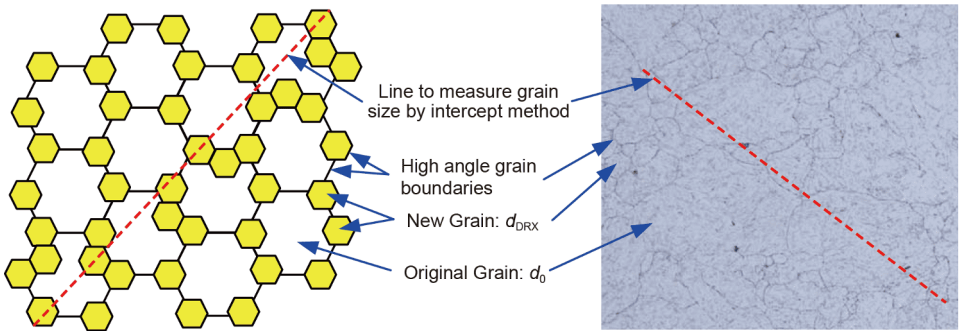

Figure 8 (Color online) Schematic of the mathematical model developed to describe the volume fraction of DRX at high strain rates.

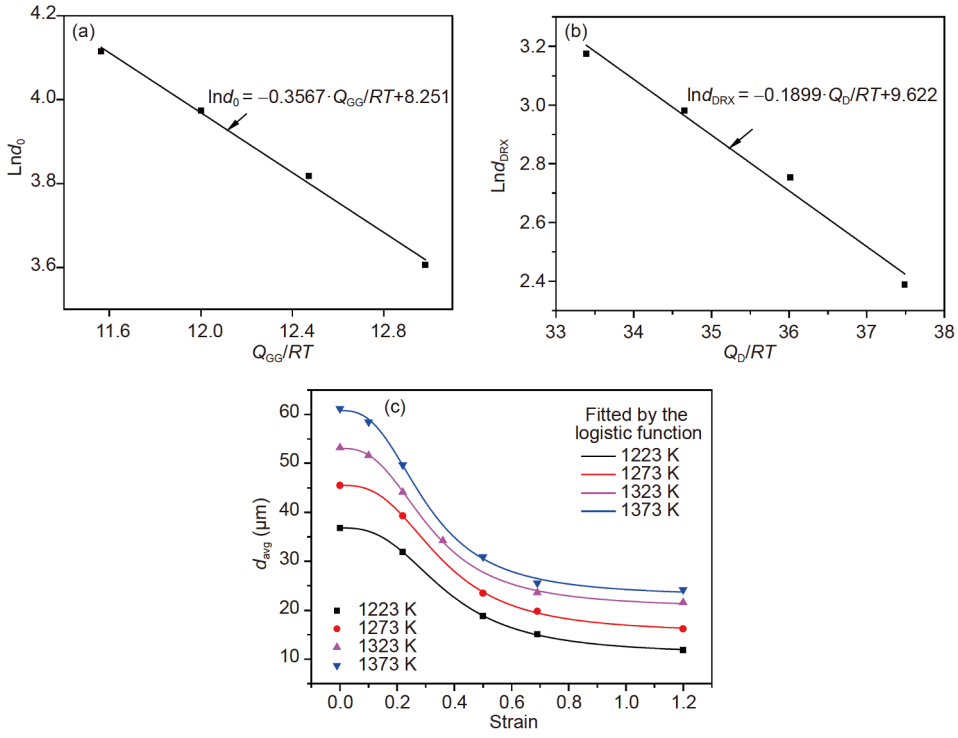

Figure 9 (Color online) Relation between: (a) d_0 and Q_{GG}/RT; (b) d_{DRX} and Q_D/RT; (c) d_{avg} and strain.

Figure 9(c) depicts the relation between average grain size d_{avg} and strain at various temperatures. It can be found that this relation can be described by a logistic function as follows:

$$d_{avg} = d_{DRX} + \frac{d_0 - d_{DRX}}{1 + \left(\frac{\varepsilon}{0.336}\right)^{2.74}}. \quad (6)$$

4.2.3 *Evaluation of DRX kinetics models*

The X_{DRX} at high strain rates can be obtained by substituting eqs. (5) and (6) into eq. (3). Generally, the present DRX volume fraction model at low strain rates is established by the Avrami equation [34]:

$$X_{DRX} = 1 - \exp\left(-k\left(\frac{\varepsilon - \varepsilon_c}{\varepsilon_p}\right)^m\right), \quad (7)$$

where X_{DRX} is the DRX volume fraction, ε_c is the critical strain, ε_p is the peak strain, and k and m are material constants. The existing DRX grain size models is established by the power law function of Z [13] and expressed as follows:

$$d_{DRX} = A \cdot Z^n, \quad (8)$$

where A and n are material constants, $Z = \dot{\varepsilon}\exp(Q_D/RT)$, and $\dot{\varepsilon}$ is the strain rate.

ε_c, ε_p, m, k, and d_{DRX} are calculated based on the data of this study by using the method proposed in refs. [30] and [13], and the corresponding expressions are as follows:

$$\begin{cases} \varepsilon_c = 4.52\times10^{-4}\cdot Z^{0.18019}, \\ \varepsilon_p = 1.59\times10^{-3}\cdot Z^{0.15562}, \\ m = 2.02, \\ k = 0.11767\cdot \ln Z - 2.68, \\ d_{DRX} = 7.65\times10^{3}\cdot Z^{-0.16}. \end{cases} \quad (9)$$

Figure 10(a) shows the microstructures at strain 1.2 and 10 s^{-1} at different temperatures, and Figure 10(b) compares the X_{DRX} calculated by the Avrami model and proposed model with the X_{DRX} obtained by experiments. Figure 10(b) shows that there are obvious differences between the X_{DRX} calculated by the Avrami model and obtained by experiments. In addition, the microstructures in Figure 10(a) exhibit that DRX is practically completed at all the temperatures, which is different from analysis of the X_{DRX} calculated by the Avrami model. Furthermore, comparing the X_{DRX} calculated by the Avrami model at 1323 K (the blue dotted line in Figure 10(b)) with the microstructures at various strains in Figure 6 shows that they are still inconsistent. Thus, the DRX critical strain in the Avrami model is approximately 0.5, but the microstructure at ε = 0.22 presented in Figure 6 shows that DRX has already started. Hence, the Avrami model cannot predict the DRX volume fraction at high strain rates. From the comparison of the X_{DRX} calculated by the proposed model as presented in Sect. 4.2.1 and obtained by experiments (see Figure 10(b)), it can be found that the former exhibits a good agreement with the latter. Moreover, the microstructures also accurately match the X_{DRX} calculated by the proposed model. In addition, comparing the calculated X_{DRX} by the model at 10 s^{-1} and 1323 K with the microstructures at different strains presented in Figure 6

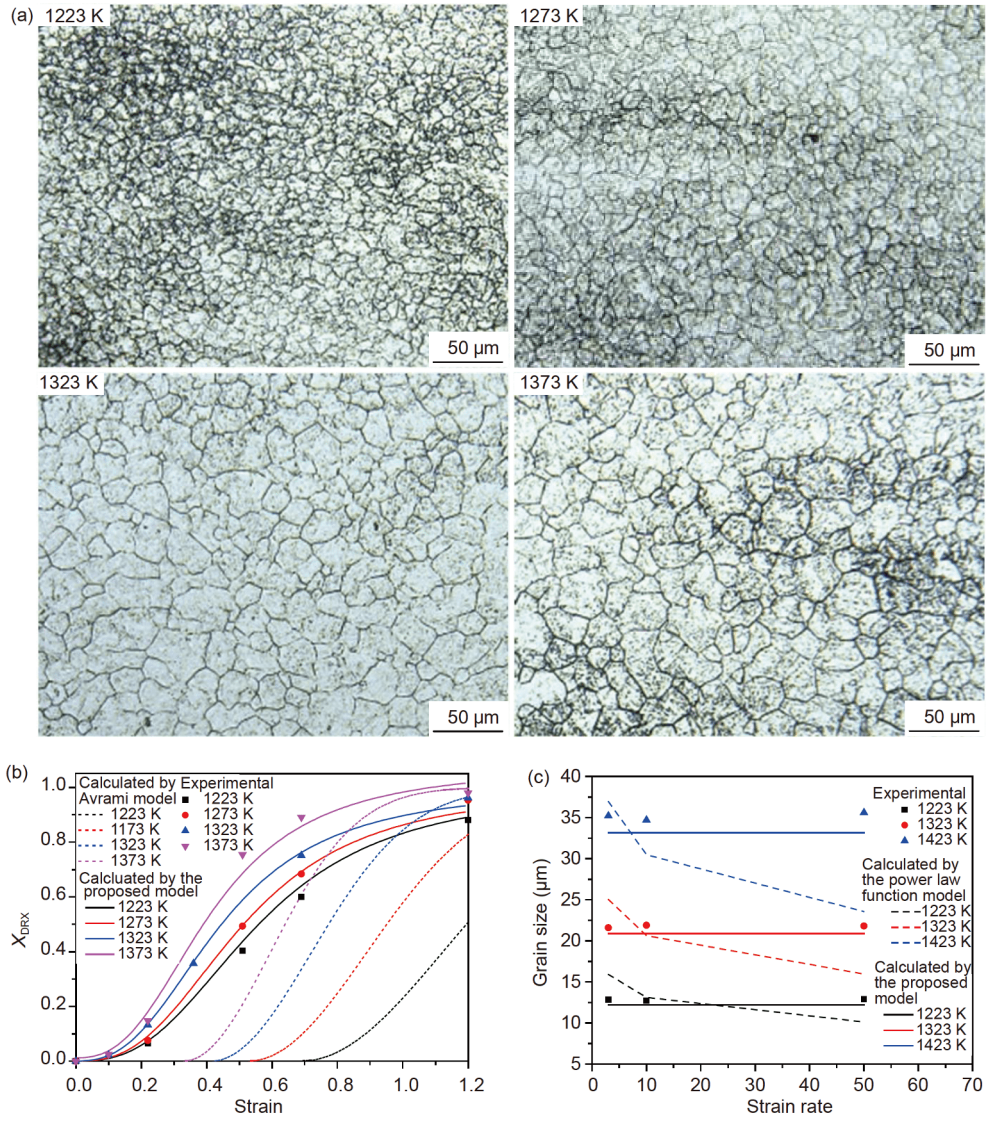

Figure 10 (Color online) Microstructures and comparisons of models with experiments: (a) microstructures at the strain of 1.2 and 10 s^{-1}; (b) comparison of the X_{DRX} calculated by the Avrami model and proposed model with the experimental data at 10 s^{-1}; (c) comparison of the grain sizes calculated by the power law function of Z and proposed model with the experimental data.

reveals that they are also well consistent. Therefore, the DRX volume fraction of 300M steel at high strain rates can be described by d_0, d_{DRX}, and d_{avg} with good precision. Figure 10(c) displays the comparison of the grain sizes calculated by the power law function model and proposed model with experimental data. It can be seen that the grain sizes obtained from experiments are significantly different from those calculated by the power law function model but exhibit a good agreement with those calculated by the proposed model. This also shows that the proposed model of the DRX grain size has an enhanced predicting accuracy.

From the results above, it can be deduced that the DRX fraction/grain size cannot be accurately predicted by the Avrami model/power law function model. When deformation occurs at high strain rates, the flow curves have no stress peaks because of the transition in the DRX mechanism, so that ε_p cannot be obtained directly from the flow curves. When the Avrami model is used to calculate the DRX fraction at high strain rates, ε_p and ε_c are calculated by eq. (9). It is inappropriate to use this method, and hence, inaccurate X_{DRX} is calculated by eq. (7). However, in the model proposed in this study, X_{DRX} is obtained using the grain sizes at different strains rather than from the flow curves. Thus, the proposed model is free from the effect of the presence or absence of a stress peak in the flow curve. Moreover, in the power law function model, the grain size is a function of the temperature and strain rate, such that the grain size decreases with the increase in the strain rate. In this study, the grain size practically remains constant in the high strain rate range. Thus, the power law function is unsuitable for describing the DRX grain size under high-strain rate deformation conditions.

5 Conclusions

In this study, the effects of the strain rate on the flow behavior and DRX mechanism of 300M steel are systematically investigated. The strain rate has more obviously effects on the flow stress and microstructures compared with those of temperature. The DSR for 300M steel calculated by the method of combining the stress ratio with the grain size is 1.8 s^{-1}. At strain rates lower than the DSR, stress peaks exist in the flow curves owing to the decrease in the dislocation density caused by the grain boundary migration. The DRX mechanism is a DDRX, and the grain size decreases with strain rate increase. In contrast, the flow curves do not exhibit a stress peak at strain rates higher than the DSR. The related DRX mechanism is a CDRX, and the grain size remains constant at the same temperature because no grain growth occurs in the limited deformation time. The DRX volume fraction model at high strain rates is established based on initial grain size d_0, DRX grain size d_{DRX}, and average grain size d_{avg}. Combined with the existing DRX kinetics models at low strain rates, the processing parameters can be optimized to control the coarse grains and inhomogeneous microstructures, thus obtaining components with excellent mechanical properties.

This work was supported by the National Natural Science Foundation for Distinguished Young Scholars of China (Grant No. 51725504), and the State Key Program of National Natural Science Foundation of China (Grant No. 51435007).

1 Chen M S, Lin Y C, Ma X S. The kinetics of dynamic recrystallization of 42CrMo steel. Mater Sci Eng-A, 2012, 556: 260–266
2 Quan G Z, Li G S, Chen T, et al. Dynamic recrystallization kinetics of 42CrMo steel during compression at different temperatures and strain rates. Mater Sci Eng-A, 2011, 528: 4643–4651
3 Liu Y X, Lin Y C, Li H B, et al. Study of dynamic recrystallization in a Ni-based superalloy by experiments and cellular automaton model. Mater Sci Eng-A, 2015, 626: 432–440
4 Yin F, Hua L, Mao H, et al. Microstructural modeling and simulation for GCr15 steel during elevated temperature deformation. Mater Des, 2014, 55: 560–573
5 Pinheiro I P, Barbosa R, Cetlin P R. The relevance of dynamic recrystallization in the hot deformation of IF steel at high strain rates. Mater Sci Eng-A, 2007, 457: 90–93
6 Dudova N, Belyakov A, Sakai T, et al. Dynamic recrystallization mechanisms operating in a Ni-20%Cr alloy under hot-to-warm working. Acta Mater, 2010, 58: 3624–3632
7 Tóth L S, Estrin Y, Lapovok R, et al. A model of grain fragmentation based on lattice curvature. Acta Mater, 2010, 58: 1782–1794
8 Luo J, Li M Q, Liu Y G, et al. The deformation behavior in isothermal compression of 300M ultrahigh-strength steel. Mater Sci Eng-A, 2012, 534: 314–322
9 Liu J, Liu Y G, Lin H, et al. The metadynamic recrystallization in the two-stage isothermal compression of 300M steel. Mater Sci Eng-A, 2013, 565: 126–131
10 Liu Y G, Luo J, Li M Q. The fuzzy neural network model of flow stress in the isothermal compression of 300M steel. Mater Des, 2012, 41: 83–88
11 Qi R, Guo B, Liu X, et al. Flow stress behaviors and microstructure evolution of 300M high strength steel under isothermal compression. J Iron Steel Res Int, 2014, 21: 1116–1123
12 Sun H M, Li M Q, Liu Y G. Development of processing map coupling grain size for the isothermal compression of 300M steel. Mater Sci Eng-A, 2014, 595: 77–85
13 Liu Y G, Li M Q, Luo J. The modelling of dynamic recrystallization in the isothermal compression of 300M steel. Mater Sci Eng-A, 2013, 574: 1–8
14 Eghbali B. Effect of strain rate on the microstructural development through continuous dynamic recrystallization in a microalloyed steel. Mater Sci Eng-A, 2010, 527: 3402–3406
15 Souza R C, Silva E S, Jorge Jr. A M, et al. Dynamic recovery and dynamic recrystallization competition on a Nb- and N-bearing austenitic stainless steel biomaterial: Influence of strain rate and temperature. Mater Sci Eng-A, 2013, 582: 96–107
16 Miura H. Strain-rate effect on dynamic recrystallization at grain boundary in Cu alloy bicrystal. Scripta Mater, 2003, 48: 1501–1505
17 Yang Q, Deng Z, Zhang Z, et al. Effects of strain rate on flow stress behavior and dynamic recrystallization mechanism of Al-Zn-Mg-Cu aluminum alloy during hot deformation. Mater Sci Eng-A, 2016, 662: 204–213
18 Jiang H, Dong J, Zhang M, et al. A study on the effect of strain rate on the dynamic recrystallization mechanism of alloy 617B. Metall Mat Trans A, 2016, 47: 5071–5087

19 Pradhan S K, Mandal S, Athreya C N, et al. Influence of processing parameters on dynamic recrystallization and the associated annealing twin boundary evolution in a nickel base superalloy. Mater Sci Eng-A, 2017, 700: 49–58
20 Garcıa de Andrés C, Bartolomé M J, Capdevila C, et al. Metallographic techniques for the determination of the austenite grain size in medium-carbon microalloyed steels. Mater Charact, 2001, 46: 389–398
21 Barraclough D R. Etching of prior austenite grain boundaries in martensite. Metallography, 1973, 6: 465–472
22 Bodnar R L, McGraw V E, Brandemarte A V. Technique for revealing prior austenite grain boundaries in CrMoV turbine rotor steel. Metallography, 1984, 17: 109–114
23 Zhang S S, Li M Q, Liu Y G, et al. The growth behavior of austenite grain in the heating process of 300M steel. Mater Sci Eng-A, 2011, 528: 4967–4972
24 Sakai T, Belyakov A, Kaibyshev R, et al. Dynamic and post-dynamic recrystallization under hot, cold and severe plastic deformation conditions. Prog Mater Sci, 2014, 60: 130–207
25 Roberts W, Ahlblon B. A nucleation criterion for dynamic recrystallization during hot working. Acta Metallurgica, 1978, 26: 801–813
26 Lin Y C, Chen X M, Wen D X, et al. A physically-based constitutive model for a typical nickel-based superalloy. Comput Mater Sci, 2014, 83: 282–289
27 Huang K, Logé R E. A review of dynamic recrystallization phenomena in metallic materials. Mater Des, 2016, 111: 548–574
28 Doherty R D, Hughes D A, Humphreys F J, et al. Current issues in recrystallization: A review. Mater Sci Eng-A, 1997, 238: 219–274
29 Hansen N, Huang X. Dislocation structures and flow stress. Mater Sci Eng-A, 1997, 234-236: 602–605
30 Zhang C, Zhang L, Xu Q, et al. The kinetics and cellular automaton modeling of dynamic recrystallization behavior of a medium carbon Cr-Ni-Mo alloyed steel in hot working process. Mater Sci Eng-A, 2016, 678: 33–43
31 Abedi H R, Zarei Hanzaki A, Liu Z, et al. Continuous dynamic recrystallization in low density steel. Mater Des, 2017, 114: 55–64
32 Yin X Q, Park C H, Li Y F, et al. Mechanism of continuous dynamic recrystallization in a 50Ti-47Ni-3Fe shape memory alloy during hot compressive deformation. J Alloys Compd, 2017, 693: 426–431
33 Ion S E, Humphreys F J, White S H. Dynamic recrystallisation and the development of microstructure during the high temperature deformation of magnesium. Acta Metall, 1982, 30: 1909–1919
34 Zhao B, Zhao T, Li G, et al. The kinetics of dynamic recrystallization of a low carbon vanadium-nitride microalloyed steel. Mater Sci Eng-A, 2014, 604: 117–121